

ESI-1

Electronic Supplemental Information File

Interfacial Molecular Restructuring of Plasticized Polymers in Water

*Jeanne M. Hankett^{‡1}, Xiaolin Lu^{‡2}, Yuwei Liu¹, Emily Seeley¹, Zhan Chen^{*1}*

[‡]These coauthors contributed equally to this article

*Corresponding author: zhanc@umich.edu

¹Department of Chemistry, University of Michigan, 930 North University Avenue, Ann Arbor,

MI 48109 USA

²State Key Laboratory of Bioelectronics, School of Biological Science & Medical Engineering,

Southeast University, Nanjing, 210096, Jiangsu Province, P. R. China

SFG System Details

The EXSPLA SFG system is composed of a pico-second Nd:YAG laser, a harmonic unit with two KD*P crystals, an optical parametric generation (OPG)/optical parametric amplification (OPA) and difference frequency generation (DFG) system based on LBO and AgGaS₂ (or GaSe) crystals and a detection system. The output of the Nd:YAG laser is a 20 Hz 20 ps 1064 nm near-IR beam. The visible input 532 nm beam for SFG experiments is generated by frequency-doubling a portion of this 1064 nm beam. The IR beam is generated from the OPG/OPA and DFG system and can be tuned from 1000 to 4300 cm⁻¹. For SFG experiments, the incident angles of the visible and the IR input are 60° and 55° with respect to the surface normal, respectively. The diameters of both input beams at the surface are about 500 μm. The SFG signal from the surface is collected by a photomultiplier tube and processed with a gated integrator.

Additional Information on SFG Signal Contributions

SFG is a coherent optical process involves two input (visible and infrared) beams and one output (sum) beam. Its output sum frequency intensity in the reflection mode can be written as¹:

$$\text{Eq. S-1 } I(\omega) = \frac{8\pi^3 \omega^2 \sec^2 \beta}{c^3 n_1(\omega_1) n_1(\omega_2) n_1(\omega)} |\chi_{eff}^{(2)}| I_1(\omega_1) I_2(\omega_2) AT$$

where β is the output sum frequency reflection angle, $n_i(\omega_i)$ is the frequency (ω_i) dependent refractive index of the medium, $I_1(\omega_1)$ and $I_2(\omega_2)$ are the intensities of the input visible and IR fields, respectively, T is the input beam pulse-width, A is the overlapping area of the two input beams at the sample surfaces or/and interfaces, and $\chi_{eff}^{(2)}$ is the effective second-order nonlinear optical susceptibility. Since each beam can be adjusted to either an s- or p-polarization, $\chi_{eff}^{(2)}$ with

different polarization combinations can be experimentally measured, such as ssp (s-polarized sum frequency signal, s-polarized visible beam, and p-polarized IR beam), sps, pss, and ppp polarization combinations.¹

$$\text{Eq. S-2 } \chi_{eff,ssp}^{(2)} = L_{yy}(\omega)L_{yy}(\omega_1)L_{zz}(\omega_2)\sin\beta_2\chi_{yyz}$$

$$\text{Eq. S-3 } \chi_{eff,sps}^{(2)} = L_{yy}(\omega)L_{zz}(\omega_1)L_{yy}(\omega_2)\sin\beta_1\chi_{zyy}$$

$$\text{Eq. S-4 } \chi_{eff,pss}^{(2)} = L_{zz}(\omega)L_{yy}(\omega_1)L_{yy}(\omega_2)\sin\beta\chi_{zyy}$$

$$\begin{aligned} \text{Eq. S-5 } \chi_{eff,ppp}^{(2)} = & -L_{xx}(\omega)L_{xx}(\omega_1)L_{zz}(\omega_2)\cos\beta\cos\beta_1\sin\beta_2\chi_{xxz} \\ & -L_{xx}(\omega)L_{zz}(\omega_1)L_{xx}(\omega_2)\cos\beta\sin\beta_1\cos\beta_2\chi_{xzx} \\ & +L_{zz}(\omega)L_{xx}(\omega_1)L_{xx}(\omega_2)\sin\beta\cos\beta_1\cos\beta_2\chi_{zxx} \\ & +L_{zz}(\omega)L_{zz}(\omega_1)L_{zz}(\omega_2)\sin\beta\sin\beta_1\sin\beta_2\chi_{zzz} \end{aligned}$$

Here in these four equations there are seven tensor components of second-order nonlinear susceptibility (χ_{yyz} , χ_{zyy} , χ_{zzy} , χ_{xxz} , χ_{xzx} , χ_{zxx} , and χ_{zzz}) within the surface-fixed coordinate system. β , β_1 and β_2 are the output angle for the sum frequency signal, input angle of the visible beam and input angle of the infrared beam, respectively. L_{ii} s are (i=x, y, or z) the Fresnel coefficients responsible for the local field correction of the two input and one output beams. For a single surface or interface embedded between two semi-infinite media, L_{ii} s can be written as¹⁻³:

$$\text{Eq. S-6 } L_{xx}(\omega) = \frac{2n_1(\omega)\cos\gamma}{n_1(\omega)\cos\gamma + n_2(\omega)\cos\beta}$$

$$\text{Eq. S-7 } L_{yy}(\omega) = \frac{2n_1(\omega)\cos\beta}{n_1(\omega)\cos\beta + n_2(\omega)\cos\gamma}$$

$$\text{Eq. S-8 } L_{zz}(\omega) = \frac{2n_2(\omega)\cos\beta}{n_1(\omega)\cos\gamma + n_2(\omega)\cos\beta} \cdot \left(\frac{n_1(\omega)}{n'(\omega)} \right)^2$$

For all the sum frequency, visible and IR beams, such equations responsible for the local field correction are valid. Here, β is the beam input or output angle and γ is the refracted angle in

the medium 2, and $n'(\omega)$ is the refractive index of the surface or interfacial layer. An SFG spectrum can be fitted using the following equation:

$$\text{Eq. S-9 } \chi_{ijk}^{(2)} = \chi_{NR} + F_{ijk} \sum_q \frac{A_q}{\omega_2 - \omega_q + i\Gamma_q}$$

Where χ_{NR} is the non-resonant background arising from the electric polarization of the surface or interface and the adjacent media, F_{ijk} is the Fresnel coefficient responsible for the local field correction, and A_q , ω_q , and Γ_q are the strength, resonant infrared frequency, and damping coefficient of the q th vibrational mode, respectively. The above descriptions related to Equations S-1 to S-9 correspond to a single surface or interface which can generate the SFG signals. However, for a polymer film with two interfaces, further discussion is needed to consider the contributions from both interfaces, as discussed in detail in the spectral deconvolution section.

Information on Film Thickness Choice

Clearly there are SFG signal interference complications that can occur at various film thicknesses, as demonstrated by the results in the main paper and the Fresnel coefficient plots found in Figures S-1 and S-2. This may bring up the question as to why we chose to use ~200 nm thick plastic film to obtain our SFG measurements. Even though we have interfacial signal interferences, the 200 nm thick film was used for several practical reasons. Firstly, this film thickness ensures that the plasticizers interact with the plastic correctly (films thinner than 100 nm may not behave as plastics, but separated plasticizer and polymer layers). Secondly, the sample preparation methods to form 200 nm films were easily reproduced, allowing for the production of films with consistent SFG signals and with consistent bulk thicknesses. Thirdly, films produced that were much thicker than 200 nm generated very low signals in window

geometry due to light scattering (the films were no longer optically flat). Therefore, a ~200 nm thick film thickness was chosen for all SFG experiments.

Spectral Deconvolution Analysis

For this paper, we performed the spectral deconvolution analysis outlined below. We deduced signal interferences from two interfaces created with prism geometry by comparing film SFG signals in air on windows to those on prisms, and applied this logic to signals obtained at the polymer/water interface as well.

We calculated the Fresnel coefficients responsible for both interfaces using a thin-film model. The calculated Fresnel coefficients plotted as a function of the polymer film thickness using ssp and ppp polarization combinations are shown in Figures S-1 (window face-down contacting air and window face-down contacting water), and S-2 (prism contacting air and prism contacting water). From such curves, we can gain important perspectives on which interface may contribute more to the collected SFG spectra and quantitatively analyze our spectra.

First we inspect the Fresnel coefficients of the window geometry. Specifically for the window face-down geometry with air as the bottom contacting medium (Figure S-1), the Fresnel coefficient of the polymer surface in air for the ssp polarization combination (~0.94) is much larger than that of the silica/polymer interface and those for the ppp polarization combination. This indicates that signals from the surface may dominate prism spectra. Additionally, we are interested in methylene and methyl functional groups, hydrophobic groups which at polymer surfaces in air generally tend to orientate more towards the surface normal than those at the polymer buried interfaces. This behavior yields a larger corresponding second-order nonlinear

susceptibility tensor component, i.e. χ_{yyz} , at polymer surfaces than that at polymer buried interfaces, and therefore a larger signal.

These two reasons explain why the ssp SFG resonant signals of hydrophobic molecular groups from the buried silica/polymer interface in window geometry can generally be considered negligible compared to those arising from the polymer surface in air. In turn, the much smaller Fresnel coefficients for the ppp polarization combination explain why no ppp resonant signals were collected for this window geometry. For the window face-down geometry with water as the bottom contacting medium (Figure S-1), the Fresnel coefficients for both ssp and ppp polarization combinations are also very small, and therefore it is understandable that no SFG resonant signals were collected.

The Fresnel coefficients of the prism geometry are quite different from those of the window geometry. If the Fresnel coefficients of the prism geometry with air as the bottom contacting medium (Figure S-2) are inspected, for the ssp polarization combination of a 200-nm-thick polymer film, the Fresnel coefficient of the silica/polymer interface (~ 2.21) is much larger than that of the polymer surface in air (~ 0.66). This indicates the collected ssp spectra of the prism geometry with air as the contacting medium are composed of both contributions from the silica/polymer interface and the polymer surface in air but the contribution from the silica/polymer interface likely prevails over that of the polymer surface in air. The Fresnel coefficient differences are the intrinsic reasons why the ssp spectral features for the window geometry with air as the bottom contacting medium (Figure 3 in main paper) and the prism geometry with air as the bottom contacting medium (Figure 4) are different.

For the ppp polarization combination in prism geometry, the Fresnel coefficient of the χ_{zzz} component for the silica/polymer interface (~ 2.40) is much larger than the seven other

coefficients, i. e. χ_{xxz} , χ_{xzx} , χ_{zxx} components for the silica/polymer interface and χ_{xxz} , χ_{xzx} , χ_{zxx} , χ_{zzz} components for the polymer surface in air. This strongly suggests that for the prism geometry with air as the contacting medium, the ppp spectrum is dominated by the χ_{zzz} second-order nonlinear susceptibility tensor component at the silica/polymer interface.

If the Fresnel coefficients of the prism geometry with water as the bottom contacting medium (Figure S-2) are inspected, for the ssp polarization combination, the Fresnel coefficient of the silica/polymer interface (~ 0.98) is much smaller than that of the polymer/water interface (~ 2.56). This indicates the collected ssp spectra from prism geometry with water as the contacting medium are composed of contributions from both the silica/polymer interface and the polymer/water interface, but the contribution from the polymer/water interface will likely prevail over that of the silica/polymer interface.

For the ppp polarization combination of a 200-nm-thick polymer film, the Fresnel coefficients of the χ_{zzz} components for both the silica/polymer interface (~ 1.15) and the polymer/water interface (~ 2.50) are much larger than the six other coefficients, i. e. χ_{xxz} , χ_{xzx} , and χ_{zxx} components for both the silica/polymer interface and the polymer/water interface. This again indicates the collected ppp spectra obtained in prism geometry with water as the contacting medium are composed of both contributions from the silica/polymer interface and the polymer/water interface but the contribution from the polymer/water interface will likely prevail over that of the silica/polymer interface since.

Whether using ssp or ppp polarization combinations for the prism geometry, only one second-order nonlinear susceptibility tensor component has substantial contribution to the collected spectrum. This makes quantitative analysis practical and feasible using both ssp and

ppp spectra. For a generated SFG spectrum of a 200-nm thick polymer thin film, the following equation was used to fit spectra that are composed of contributions from two interfaces:

$$\text{Eq. 1 } I_{SFG} \propto \left| \chi_{eff,ijk} \right|^2 = \left| \chi_{NR} + F_{ijk,interface1} \sum_q \frac{A_q e^{i\alpha}}{\omega - \omega_q + i\Gamma_q} + F_{ijk,interface2} \sum_q \frac{B_q}{\omega - \omega_q + i\Gamma_q} \right|^2$$

Here χ_{NR} is the non-resonant background, ω_q and Γ_q are the resonant infrared frequency and damping coefficient of the q_{th} vibrational mode, respectively, and A_q and B_q are the strengths of the q_{th} vibrational mode at the two interfaces, respectively. Once spectral peaks are fitted, generated A_q/Γ_q ratios are directly correlated to $\chi^{(2)}_{eff}$ and are therefore directly related to the observed signals. Therefore, we can directly correlate the relative A_q/Γ_q ratios to the relative contributions of a functional group at two different interfaces.³⁻¹⁰

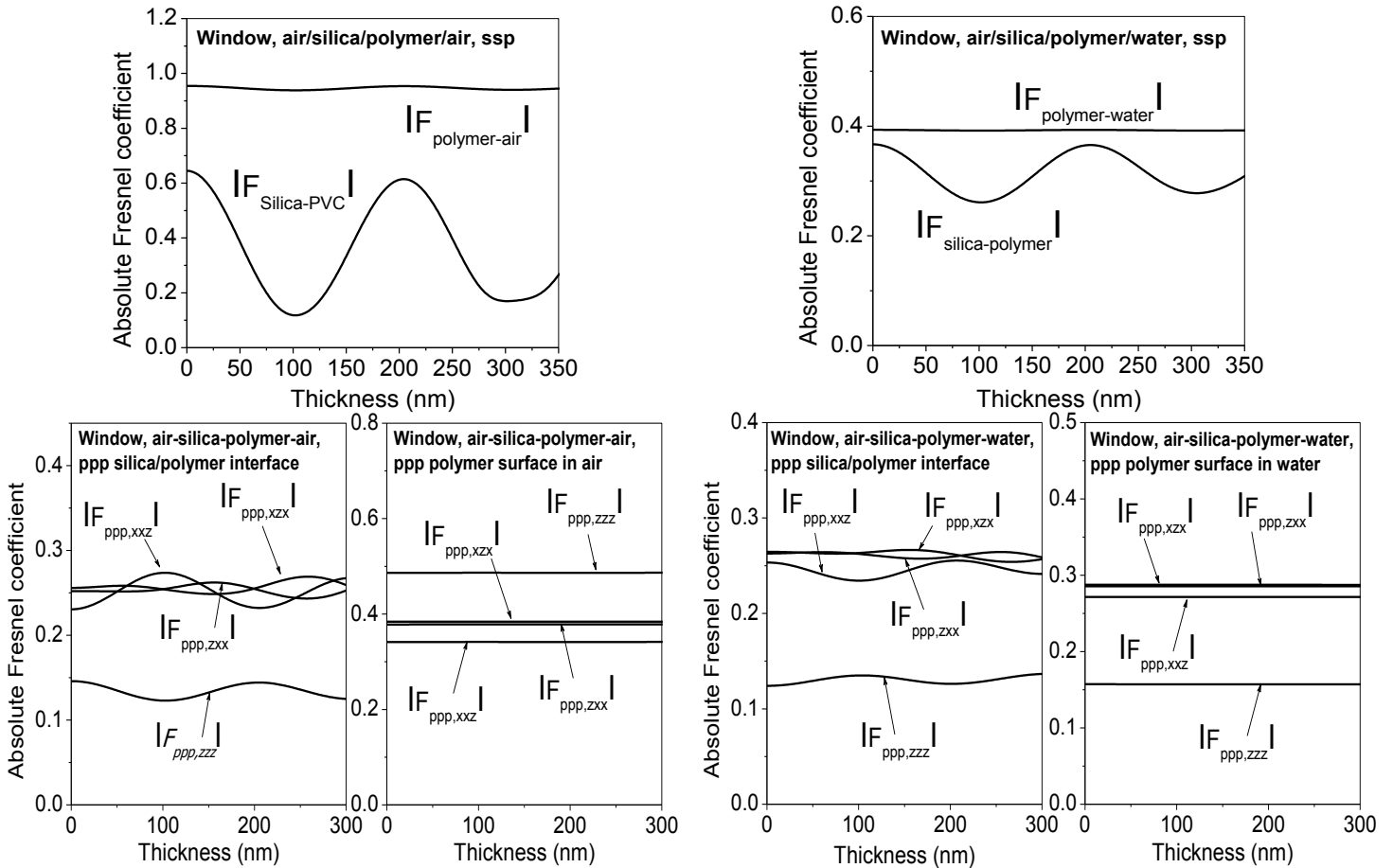


Figure S-1. (Left) The calculated Fresnel coefficients for the window face-down geometry with air as the bottom contacting medium. (Right) The calculated Fresnel coefficients for the window face-down geometry with water as the bottom contacting medium.

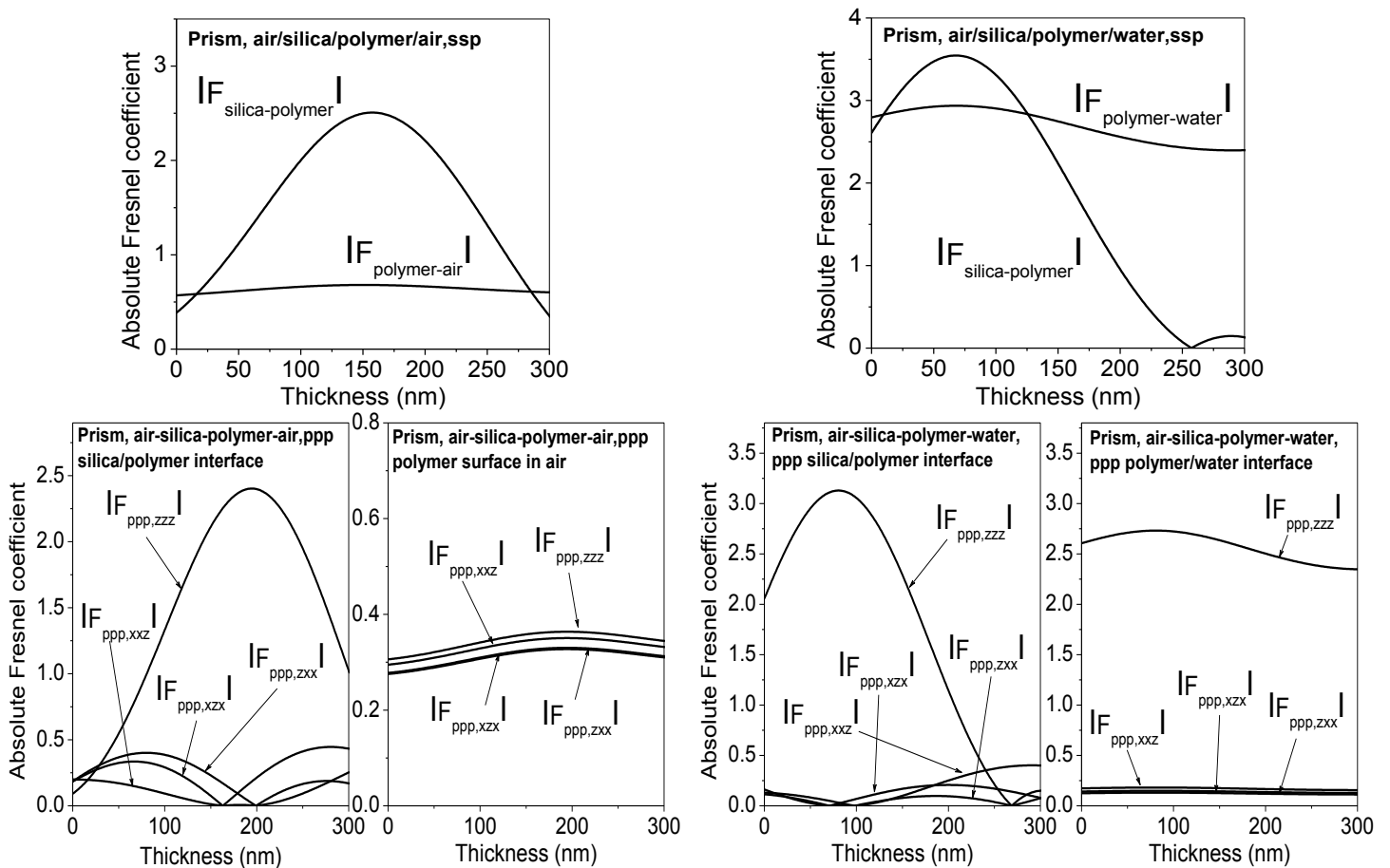


Figure S-2. (Left) The calculated Fresnel coefficients for the prism geometry with air as the bottom contacting medium. (Right) The calculated Fresnel coefficients for the prism geometry with water as the bottom contacting medium.

SFG Peak Fits

SFG prism peak fitting shown in the main paper in Figures 3-7 can be observed in detail below.

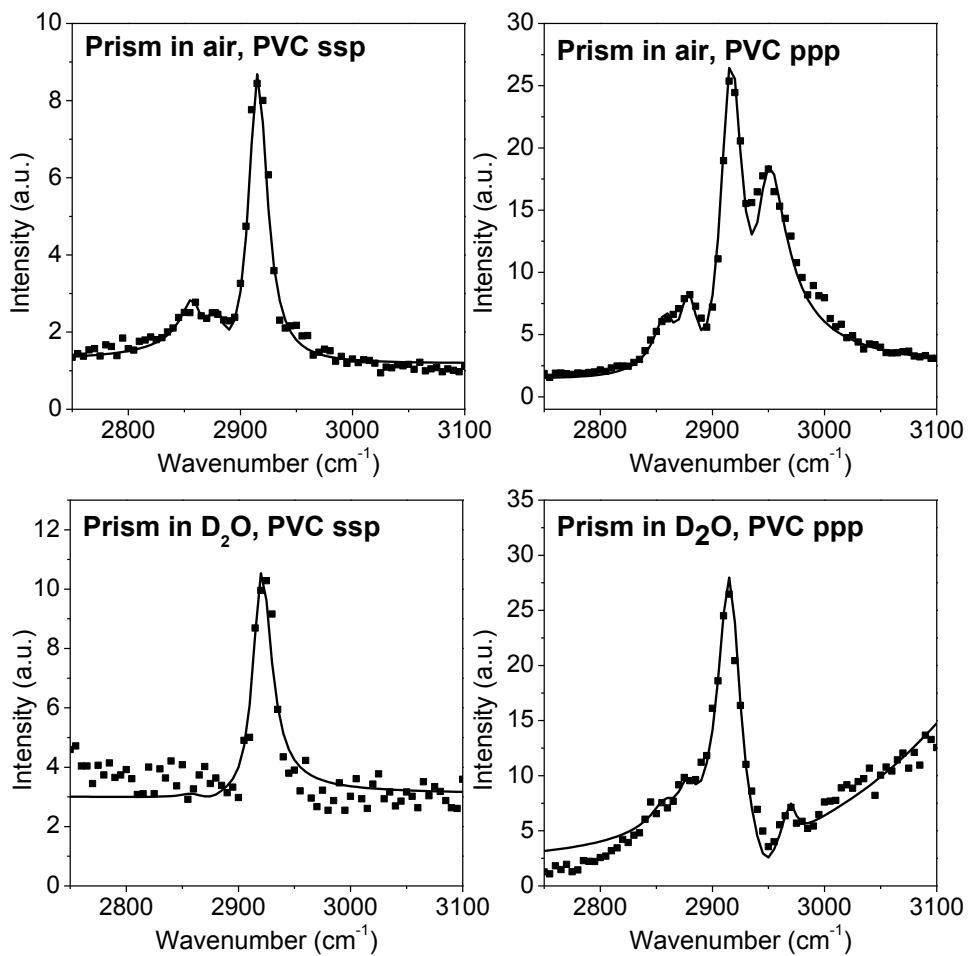


Figure S-3. Top: fitted ssp (right) and ppp (left) spectra of PVC in air on silica prisms. Fitting results are given in Table S-2. Bottom: fitted ssp (right) and ppp (left) prism spectra of PVC in D₂O upon first contact. Fitting results are given in Table S-3.

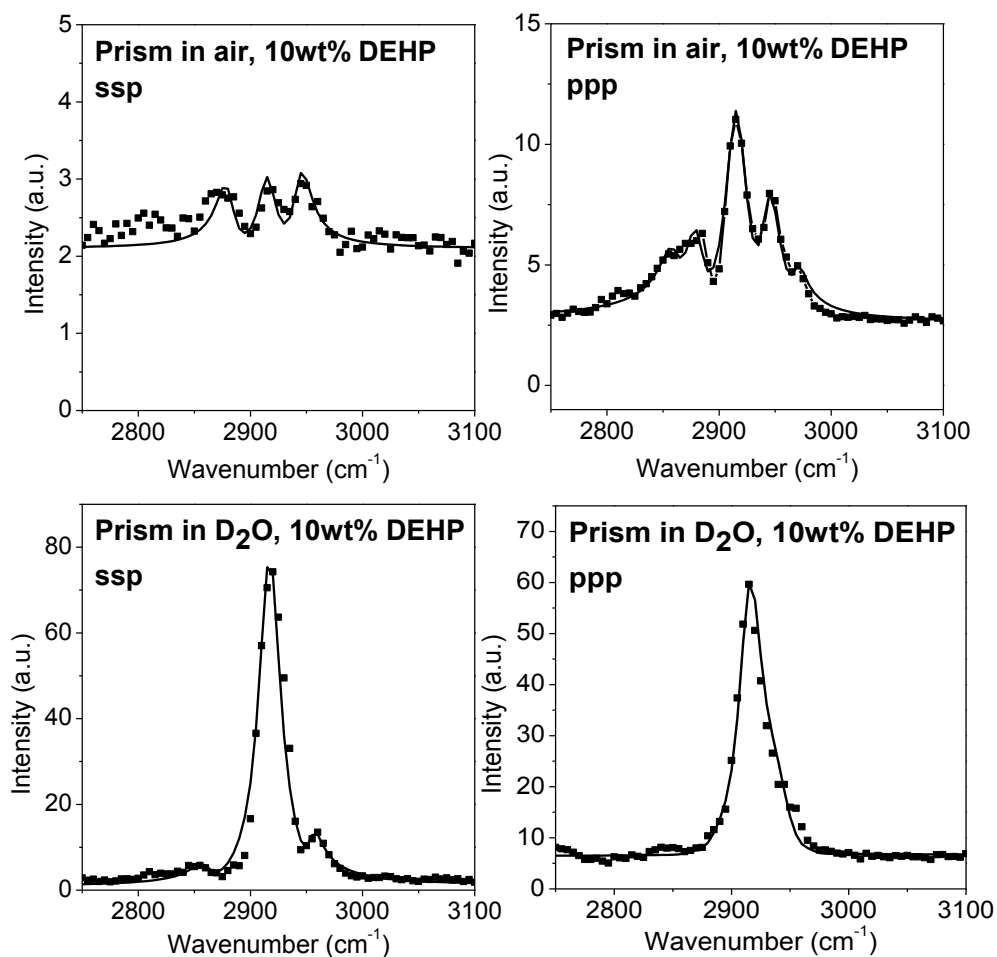


Figure S-4. Top: fitted ssp (right) and ppp (left) spectra of 10 wt% DEHP samples in air on silica prisms. Fitting results are given in Table S-5. Bottom: fitted ssp (right) and ppp (left) prism spectra of 10 wt% DEHP in D₂O upon first contact. Fitting results are given in Table S-6.

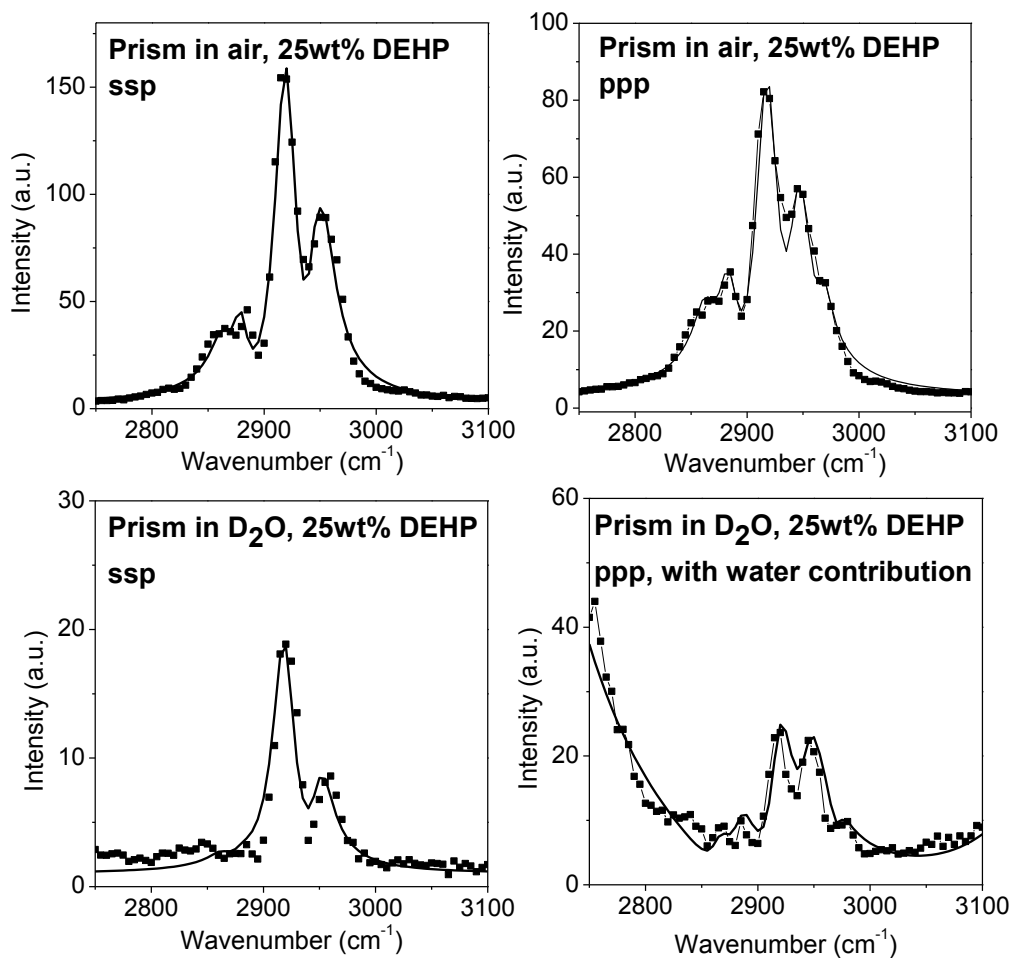


Figure S-5. Top: fitted ssp (right) and ppp (left) spectra of 25 wt% DEHP samples in air on silica prisms. Fitting results are given in Table S-8. Bottom: fitted ssp (right) and ppp (left) prism spectra of 25 wt% DEHP in D₂O upon first contact. Fitting results are given in Table S-9.

Peak Fitting Quantitative Results

Table S-1. Spectral fitting results for PVC in air in window geometry

<u>Window in air, PVC, ssp</u>						
<i>Assignment</i>	PVC surface in air			PVC/silica interface		
	<i>Wavenumber (cm⁻¹)</i>	<i>A_q</i>	<i>Γ_q</i>	<i>Wavenumber (cm⁻¹)</i>	<i>A_q</i>	<i>Γ_q</i>
CH/CH ₂	2860	-	-	-	-	-
CH ₃ (s)	2880	17	10	-	-	-
CH ₂ (s)	2915	40	10	-	-	-
CH ₂ (as)	2950	-	-	-	-	-
Fitting Details: $F_{\text{ssp,yyz}}=0.95$, $\chi_{\text{NR}}=-0.4$						

Table S-2. Spectral fitting results for PVC in air in prism geometry for ssp polarization (left) and ppp polarization (right) combinations

<u>Prism in air, PVC, ssp</u>							<u>Prism in air, PVC, ppp</u>						
<i>Assignment</i>	PVC surface in air			PVC/silica interface			<i>Assignment</i>	PVC surface in air			PVC/silica interface		
	<i>Wavenumber (cm⁻¹)</i>	<i>A_q</i>	<i>Γ_q</i>	<i>Wavenumber (cm⁻¹)</i>	<i>A_q</i>	<i>Γ_q</i>		<i>Wavenumber (cm⁻¹)</i>	<i>A_q</i>	<i>Γ_q</i>	<i>Wavenumber (cm⁻¹)</i>	<i>A_q</i>	<i>Γ_q</i>
CH/CH ₂	2860	-	-	2860	3	10	CH/CH ₂	2860	-	-	2860	5	10
CH ₃ (s)	2880	17	10	2880	-2	10	CH ₃ (s)	2880	-	-	2880	7	10
CH ₂ (s)	2915	40	10	2915	-	-	CH ₂ (s)	2915	-	-	2915 (2916)	22	12
CH ₂ (as)	2950	-	-	2950	-	-	CH ₂ (as)	2950	-	-	2950 (2947)	16	15
200 nm, $F_{\text{PVC/Air}}=0.66$, $F_{\text{Silica/PVC}}=2.21$, $\chi_{\text{nr}}=-0.2$							200 nm, $F_{\text{Silica/PVC}}=2.40$, $\chi_{\text{nr}}=0.25$						

Table S-3. Spectral fitting results for PVC in D₂O in prism geometry for ssp polarization (left) and ppp polarization (right) combinations

<u>Prism in D₂O, PVC, ssp</u>							<u>Prism in D₂O, PVC, ppp</u>						
<i>Assign- ment</i>	PVC/water interface			PVC/silica interface			<i>Assign- ment</i>	PVC/water interface			PVC/silica interface		
	<i>Wavenumber (cm⁻¹)</i>	<i>A_q</i>	<i>Γ_q</i>	<i>Wavenumber (cm⁻¹)</i>	<i>A_q</i>	<i>Γ_q</i>		<i>Wavenumber (cm⁻¹)</i>	<i>A_q</i>	<i>Γ_q</i>	<i>Wavenumber (cm⁻¹)</i>	<i>A_q</i>	<i>Γ_q</i>
CH/CH ₂	2860	-	-	2860	3	10	CH/CH ₂	2860	-3.9	10	2860	5.1	10
CH ₃ (s)	2880	-	-	2880	-2	10	CH ₃ (s)	2880	-6.0	10	2880	7.0	10
CH ₂ (s)	2915 (2919)	29	10	2915	-	-	CH ₂ (s)	2915 (2916)	-29	12	2915 (2916)	22	12
CH ₂ (as)	2950	-	-	2950	-	-	CH ₂ (as)	2950	-	-	2950 (2947)	16	15
							CHCl	2970	-2.3	10	2970	-	-
							OH	3200	-320	170	3200	-	-
200 nm, F _{PVC/Water} =2.56, F _{Silica/PVC} =0.95, χ _{NR} =0.1, α=-0.11, β=0							F _{PVC/Water} = 2.50, F _{Silica/PVC} =1.15, χ _{NR} =0.4, α= -0.11, β=3.14						

Table S-4. Spectral fitting results for 10 wt% in air in window geometry

<u>Window in air, 10 wt% DEHP, ssp</u>						
<i>Assignment</i>	10 wt% DEHP surface in air			plastic/silica interface		
	<i>Wavenumber (cm⁻¹)</i>	<i>A_q</i>	<i>Γ_q</i>	<i>Wavenumber (cm⁻¹)</i>	<i>A_q</i>	<i>Γ_q</i>
CH/CH ₂ (PVC)	2860	-	-	-	-	-
CH ₃ (s) (PVC)	2880	-	-	-	-	-
CH ₂ (s) (PVC)	2915	21	10	-	-	-
CH ₂ (as) (PVC)	2950	-	-	-	-	-
CH ₂ (s) (DEHP)	2860	-	-	-	-	-
CH ₃ (s) (DEHP)	2880	15	10	-	-	-
CH ₃ (Fermi) (DEHP)	2945	14	10	-	-	-
200 nm, F _{ssp,yyz} =0.95, χ _{nr} =-0.4						

Table S-5. Spectral fitting results for 10 wt% DEHP in air in prism geometry for ssp polarization (left) and ppp polarization (right) combinations

<u>Prism in air, 10 wt% DEHP, ssp</u>							<u>Prism in air, 10 wt% DEHP, ppp</u>						
<i>Assignment</i>	10 wt% DEHP surface in air			plastic/silica interface			<i>Assignment</i>	10 wt% DEHP surface in air			plastic/silica interface		
	<i>Wavenumber (cm⁻¹)</i>	<i>A_q</i>	<i>Γ_q</i>	<i>Wavenumber (cm⁻¹)</i>	<i>A_q</i>	<i>Γ_q</i>		<i>Wavenumber (cm⁻¹)</i>	<i>A_q</i>	<i>Γ_q</i>	<i>Wavenumber (cm⁻¹)</i>	<i>A_q</i>	<i>Γ_q</i>
CH/CH ₂ (PVC)	2860	-	-	-	-	-	CH/CH ₂ (PVC)	2860	-	-	2860	2.8	10
CH ₃ (s) (PVC)	2880	-	-	-	-	-	CH ₃ (s) (PVC)	2880	-	-	-	-	-
CH ₂ (s) (PVC)	2915	21	10	2915	-3.3	12	CH ₂ (s) (PVC)	2915	-	-	2915 (2916)	13	12
CH ₂ (as) (PVC)	2950	-	-	-	-	-	CH ₂ (as) (PVC)	2950	-	-	-	-	-
CH ₂ (s) (DEHP)	2860	-	-	-	-	-	CH ₂ (s) (DEHP)	2860	-	-	-	-	-
CH ₃ (s) (DEHP)	2880	15	10	2880	-1.0	10	CH ₃ (s) (DEHP)	2880	-	-	2880 (2881)	4.9	10
CH ₃ (Fermi) (DEHP)	2945	14	10	2945 (2944)	-0.7	10	CH ₃ (Fermi) (DEHP)	2945	-	-	2945 (2944)	6.6	10
							CHCl (PVC)				2970 (2969)	1.6	7
F _{PVC/Air} =0.66, F _{Silica/PVC} =2.21, χ _{nr} =0, β=0, α=0							F _{PVC/Air} =0.36, F _{Silica/PVC} =2.40, χ _{nr} =0.4, β=3.14, α=-0.11						

Table S-6. Spectral fitting results for 10 wt% DEHP in D₂O in prism geometry for ssp polarization (left) and ppp polarization (right) combinations

<u>Prism in D₂O, 10 wt% DEHP, ssp</u>							<u>Prism in D₂O, 10 wt% DEHP, ppp</u>						
<i>Assignment</i>	10 wt% DEHP/water interface			plastic/silica interface			<i>Assignment</i>	10 wt% DEHP/water Interface			plastic/silica interface		
	<i>Wavenumber (cm⁻¹)</i>	<i>A_q</i>	<i>Γ_q</i>	<i>Wavenumber (cm⁻¹)</i>	<i>A_q</i>	<i>Γ_q</i>		<i>Wavenumber (cm⁻¹)</i>	<i>A_q</i>	<i>Γ_q</i>	<i>Wavenumber (cm⁻¹)</i>	<i>A_q</i>	<i>Γ_q</i>
CH/CH ₂ (PVC)	2860	4.0	10	2860	-	-	CH/CH ₂ (PVC)	2860	-	-	2860	2.8	10
CH ₃ (s) (PVC)	2880	-	-	-	-	-	CH ₃ (s) (PVC)	2880	-	-	-	-	-
CH ₂ (s) (PVC)	2915 (2917)	42	12	2915 (2916)	-3.3	12	CH ₂ (s) (PVC)	2915	-42	12	2915 (2916)	13.1	12
CH ₂ (as) (PVC)	2950	-	-	-	-	-	CH ₂ (as) (PVC)	2950	10	15	-	-	-
CH ₂ (s) (DEHP)	2860	-	-	-	-	-	CH ₂ (ss) (DEHP)	2860	-	-	-	-	-
CH ₃ (s) (DEHP)	2880	-	-	2880 (2881)	-1.0	10	CH ₃ (s) (DEHP)	2880	-	-	2880 (2881)	4.9	10
CH ₃ (Fermi) (DEHP)	2945	-	-	2945 (2944)	-0.7	10	CH ₃ (Fermi) (DEHP)	2945	-	-	2945 (2944)	6.6	10
Unassigned	2955	3.8	7	2955	-	-	CHCl (PVC)	2970	-	-	2970	1.6	7
F _{PVC/Water} =2.56, F _{Silica/PVC} =0.95, χ _{nr} =0.1, β=0, α=-0.11							F _{PVC/Water} =2.50, F _{Silica/PVC} =1.15χ _{nr} =0.1, β=3.14, α=-0.11						

Table S-7. Spectral fitting results for 25 wt% DEHP in air in window geometry

<u>Window in air, 25 wt% DEHP, ssp</u>						
<i>Assignment</i>	25 wt% DEHP surface in air			plastic/silica interface		
	<i>Wavenumber (cm⁻¹)</i>	<i>A_q</i>	<i>Γ_q</i>	<i>Wavenumber (cm⁻¹)</i>	<i>A_q</i>	<i>Γ_q</i>
CH/CH ₂ (PVC)	2860	-	-	-	-	-
CH ₃ (s) (PVC)	2880	-	-	-	-	-
CH ₂ (s) (PVC)	2915	-20	10	-	-	-
CH ₂ (as) (PVC)	2950	-	-	-	-	-
CH ₂ (s) (DEHP)	2860 (2865)	10	10	-	-	-
CH ₃ (s) (DEHP)	2880	24	7	-	-	-
CH ₃ (Fermi) (DEHP)	2945 (2944)	23	7	-	-	-
200 nm, F _{ssp,yyz} =0.95, χ _{nr} =-0.4						

Table S-8. Spectral fitting results for 25 wt% DEHP in air in prism geometry for ssp polarization (left) and ppp polarization (right) combinations

<u>Prism in air, 25wt% DEHP, ssp</u>							<u>Prism in air, 25 wt% DEHP, ppp</u>						
<i>Assignment</i>	25 wt% DEHP surface in air			plastic/silica interface			<i>Assignment</i>	25 wt% DEHP surface in air			plastic/silica interface		
	<i>Wavenumber (cm⁻¹)</i>	<i>A_q</i>	<i>Γ_q</i>	<i>Wavenumber (cm⁻¹)</i>	<i>A_q</i>	<i>Γ_q</i>		<i>Wavenumber (cm⁻¹)</i>	<i>A_q</i>	<i>Γ_q</i>	<i>Wavenumber (cm⁻¹)</i>	<i>A_q</i>	<i>Γ_q</i>
CH/CH ₂ (PVC)	2860	0	-	-	-	-	CH/CH ₂ (PVC)	2860	-	-	-	-	-
CH ₃ (s) (PVC)	2880	0	-	-	-	-	CH ₃ (s) (PVC)	2880	-	-	-	-	-
CH ₂ (s) (PVC)	2915	-20	10	2915 (2919)	68	12	CH ₂ (s) (PVC)	2915	-	-	2915 (2918)	39	12
CH ₂ (as) (PVC)	2950	0	-	-	-	-	CH ₂ (as) (PVC)	2950	-	-	-	-	-
CH ₂ (s) (DEHP)	2860 (2865)	10	10	2860 (2865)	5.9	10	CH ₂ (s) (DEHP)	2860 (2865)	-	-	2860 (2865)	7.3	10
CH ₃ (s) (DEHP)	2880	24	7	2880 (2883)	8.0	12	CH ₃ (s) (DEHP)	2880	-	-	2880 (2885)	17	12
CH ₃ (Fermi) (DEHP)	2944	23	7	2945 (2950)	28	12	CH ₃ (Fermi) (DEHP)	2944	-	-	2945	25	12
							CHCl (PVC)	2967	-	-	2967	4	7
F _{PVC/Air} =0.66, F _{Silica/PVC} =2.21, α=0, β=0, χ _{NR} =0							200 nm, F _{PVC/Air} =0.36, F _{Silica/PVC} =2.40, α=-0.11, β=0, χ _{nr} =0						

Table S-9. Spectral fitting results for 25 wt% DEHP in D₂O in prism geometry for ssp polarization (left) and ppp polarization (right) combinations

<u>Prism in D₂O, 25 wt% DEHP, ssp</u>							<u>Prism in D₂O, 25 wt% DEHP, ppp</u>						
<i>Assignment</i>	25 wt% DEHP/water interface			plastic/silica interface			<i>Assignment</i>	25 wt% DEHP/water interface			plastic/silica interface		
	<i>Wavenumber (cm⁻¹)</i>	<i>A_q</i>	<i>Γ_q</i>	<i>Wavenumber (cm⁻¹)</i>	<i>A_q</i>	<i>Γ_q</i>		<i>Wavenumber (cm⁻¹)</i>	<i>A_q</i>	<i>Γ_q</i>	<i>Wavenumber (cm⁻¹)</i>	<i>A_q</i>	<i>Γ_q</i>
CH/CH ₂ (PVC)	2860	-	-	-	-	-	CH/CH ₂ (PVC)	2860	-	-	-	-	-
CH ₃ (s) (PVC)	2880	-	-	-	-	-	CH ₃ (s) (PVC)	2880	-	-	-	-	-
CH ₂ (s) (PVC)	2915 (2919)	-7	-	2915 (2919)	68	12	CH ₂ (s) (PVC)	2915 (2918)	-3.3	12	2915 (2918)	39	12
CH ₂ (as) (PVC)	2950	0	-	-	-	-	CH ₂ (as) (PVC)	2950	-	-	-	-	-
CH ₂ (s) (DEHP)	2860 (2865)	-1	-	2860 (2865)	5.9	10	CH ₂ (s) (DEHP)	2860	-	-	2860 (2865)	7.3	10
CH ₃ (s) (DEHP)	2880 (2885)	-1	-	2880 (2885)	8.0	12	CH ₃ (s) (DEHP)	2880 (2885)	-1.2	12	2880 (2885)	17	12
CH ₃ (Fermi) (DEHP)	2944 (2950)	-2	-	2945(2950)	28	12	CH ₃ (Fermi) (DEHP)	2945	-2.5	12	2945	25	12
							Unassigned	2967	-3.2	7	2967	4	7
							CHCl (PVC)	2975	1.0	7	2975	-	-
							O-D vibration	2570	600	50	2570	-	-
							O-H vibration	3200	200	100	3200	-	-
F _{PVC/Water} =2.56, F _{Silica/PVC} =0.95, α=-0.11, β=0, χ _{nr} =0.0							F _{PVC/Air} =2.50, F _{Silica/PVC} =1.15, α=-0.11, β=0, χ _{nr} =0						

FTIR Experiments

For FTIR experiments, calcium fluoride windows (ESCO Products, Inc.) were used in place of silica windows. Calcium fluoride windows were cleaned using Contrex detergent and deionized water, dried with nitrogen gas, cleaned using the glow discharge air plasma, and films were formed identically to silica windows and prisms. Samples were contacted to D₂O in the exact same manner as regular SFG experiments. Again, samples were allowed to dry in air for 1 h. IR spectra were taken of the samples before D₂O exposure and again after exposure with 1 h of drying time. To trap any remaining D₂O in films after the 1 h drying time, a second clean substrate was used to sandwich the polymer films. Two calcium fluoride windows were used for the background spectral file.

FTIR Instrumentation

A Nicolet 6700 FTIR spectrometer was used to determine whether or not remaining D₂O was trapped in PVC films after exposure to D₂O. The FTIR sample stage was purged with nitrogen prior to and during obtaining sample spectra to reduce water content present in the atmosphere. Pure PVC films were compared to FTIR PVC reference spectra. Spectra were obtained from 100 cm⁻¹ to 4000 cm⁻¹. Spectra are shown in a range of 3600-1000 cm⁻¹ for image clarity.

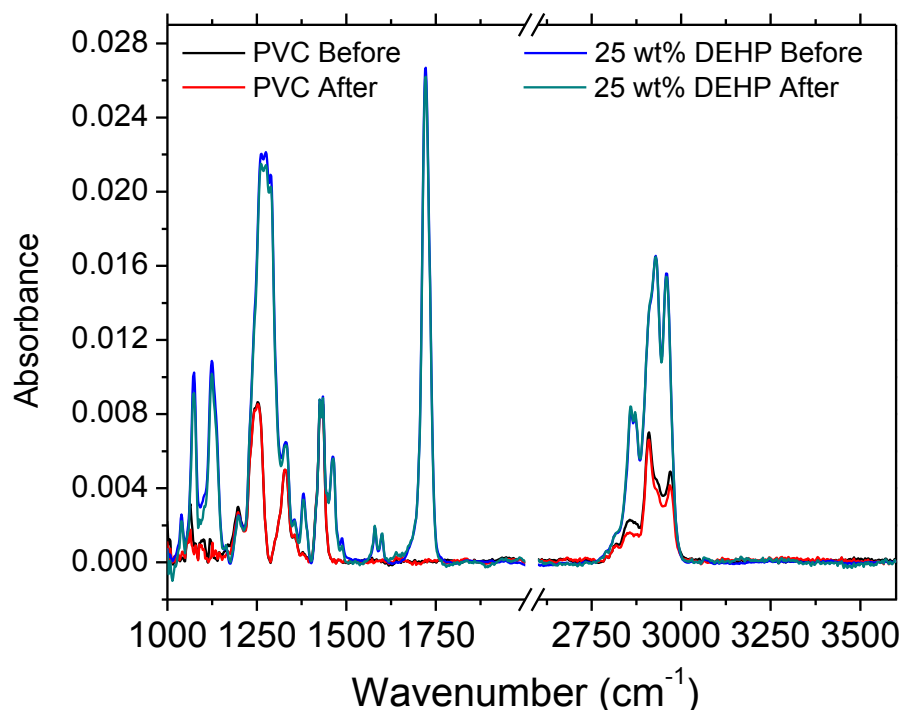


Figure S-6. FTIR spectra obtained before and after water contact for pure PVC (black and red lines, respectively) and 25 wt% DEHP (blue and green lines, respectively).

FTIR Data Analysis Discussion

First looking at FTIR spectra of the 25 wt% DEHP plasticized sample, it is obvious that not many spectral changes are observed between spectra obtained before and after water contact and air drying. Therefore, the amount of DEHP that leached from the sample was too small to observe with FTIR. Interestingly, in the lower frequency region for pure PVC, hardly any signal differences are observed before and after water contact, but there are some obvious signal intensity differences across the CH region of spectra. There are two likely scenarios for the decrease of CH signals. It is possible that some small contaminants or smaller fragments of PVC chains were removed from water contact. And/or, the process of water penetrating the PVC film changed the density of the film itself, yielding slightly different FTIR signals.

References

1. Zhuang, X.; Miranda, P.B.; Kim, D.; Shen, Y.R. Mapping Molecular Orientation and Conformation at Interfaces by Surface Nonlinear Optics. *Phys. Rev. B* **1999**, *59*, 12632-12640.
2. Shen, Y.R. Optical Second Harmonic Generation at Interfaces. *Annu. Rev. Phys. Chem.* **1989**, *40*, 327-350.
3. Feller, M. B.; Chen, W.; Shen, Y. R. Investigation of Surface-Induced Alignment of Liquid-Crystal Molecules by Optical 2nd-Harmonic Generation. *Phys. Rev. A* **1991**, *43*, 6778-6792.
4. Wilk, D.; Johannsmann, D.; Stanners, C.; Shen, Y. R. 2nd-Harmonic Generation from C-60 Thin-Films at 1.064-Mu-M. *Phys. Rev. B* **1995**, *51*, 10057-10067.
5. Lambert, A. G.; Neivandt, D. J.; Briggs, A. M.; Usadi, E. W.; Davies, P. B. Enhanced Sum Frequency Generation from a Monolayer Adsorbed on a Composite Dielectric/Metal Substrate. *J. Phys. Chem. B* **2002**, *106*, 10693-10700.
6. McGall, S. J.; Davies, P. B.; Neivandt, D. J. Interference Effects in Sum Frequency Vibrational Spectra of Thin Polymer Films: An Experimental and Modeling Investigation. *J. Phys. Chem. B* **2004**, *108*, 16030-16039.
7. Tong, Y. J.; Zhao, Y. B.; Li, N.; Osawa, M.; Davies, P. B.; Ye, S. Interference Effects in the Sum Frequency Generation Spectra of Thin Organic Films I. Theoretical Modeling and Simulation. *J. Chem. Phys.* **2010**, *133*, 034704.
8. Tong, Y. J.; Zhao, Y. B.; Li, N.; Ma, Y. S.; Osawa, M.; Davies, P. B.; Ye, S. Interference Effects in the Sum Frequency Generation Spectra of Thin Organic Films. II: Applications to Different Thin-Film Systems. *J. Chem. Phys.* **2010**, *133*, 034705.
9. Lu, X. L.; Clarke, M. L.; Li, D. W.; Wang, X. P.; Xue, G.; Chen, Z. A Sum Frequency Generation Vibrational Study of the Interference Effect in Poly(N-Butyl Methacrylate) Thin Films Sandwiched between Silica and Water. *J. Phys. Chem. C* **2011**, *115*, 13759-13767.
10. Backus, E. H. G.; Garcia-Araez, N.; Bonn, M.; Bakker, H. J. On the Role of Fresnel Factors in Sum-Frequency Generation Spectroscopy of Metal-Water and Metal-Oxide-Water Interfaces. *J. Phys. Chem. C* **2012**, *116*, 23351-23361.